Article

Formation of Metastability of Pore Gas Hydrates in Frozen Sediments: Experimental Evidence

Evgeny Chuvilin [1,*] **, Dinara Davletshina** [1,2]**, Boris Bukhanov** [1] **, Aliya Mukhametdinova** [1] **and Vladimir Istomin** [1]

[1] Center for Petroleum Science and Engineering, Skolkovo Institute of Science and Technology (Skoltech), Skolkovo Innovation Center, 121205 Moscow, Russia
[2] Sadovsky Institute of Geosphere Dynamics, 119334 Moscow, Russia
[*] Correspondence: e.chuvilin@skoltech.ru

Abstract: The Arctic permafrost and zones of hydrate stability may evolve to the conditions that allow gas hydrates to remain metastable for a long time due to self-preservation within 150 m depths. The behavior of relict (metastable) gas hydrates in frozen sediments is controlled externally by pressure and temperature and internally by the properties of hydrate particles and sediments. The sensitivity of the dissociation and self-preservation of pore gas hydrates to different factors is investigated in laboratory experiments. The observations focus on time-dependent changes in methane hydrate saturation in frozen sand samples upon the pressure dropping below phase equilibrium in the gas–hydrate–ice system. The preservation of pore gas hydrates in these conditions mainly depends on the initial hydrate and ice saturation, clay contents and mineralogy, salinity, and texture of sediments, which affect the size, shape, and structure distortion of hydrate inclusions. The self-preservation mechanism works well at high initial contents of pore ice and hydrate, low salinity, relatively low percentages of clay particles, temperatures below -4 °C, and below-equilibrium pressures. Nuclear magnetic resonance (NMR) measurements reveal considerable amounts of unfrozen pore water in frozen sediments that may hold for several days after the pressure drop, which controls the dissociation and self-preservation processes. Metastable gas hydrates in frozen sand may occupy up to 25% of the pore space, and their dissociation upon permafrost thawing and pressure drops may release up to 16 m^3 of methane into the atmosphere per 1 m^3 of hydrate-bearing permafrost.

Keywords: Arctic; permafrost; gas hydrate; experimental modelling; porous media; dissociation; self-preservation; NMR; unfrozen water; methane emission

1. Introduction

The first evidence that natural gas hydrates may exist in permafrost appeared almost fifty years ago, but they still remain poorly investigated [1,2]. The reason is primarily that they share much physical similarity with ice [3] and are hard to identify and study with conventional geophysical methods (e.g., seismic reflection profiling). Gas hydrates were recovered in cores during exploratory drilling in Arctic oil and gas fields, and their presence within the upper 150 m of permafrost was inferred from proxy markers [4,5]. Experiments [6,7] show that intrapermafrost gas hydrates may preserve in the metastable state above the present boundary of the hydrate stability zone. They arose under favorable conditions in the past, became metastable over the course of later paleoclimatic events and permafrost evolution, and have survived until now due to self-preservation at negative temperatures. The self-preservation mechanism decelerates or almost completely stops the dissociation of gas hydrates triggered by the pressure dropping below the triple phase equilibrium in the 'gas–hydrate–ice' system, due to the formation of an ice coat on gas hydrate particles at <0 °C temperatures [8]. The effect was discovered and described in 1986–1992 independently by Canadian and Russian scientists from the National Research Center in Ottawa, the VNIIGAZ Research Institute in Moscow, and the Lomonosov Moscow University [9–15].

The first Russian data on the behavior of methane hydrate and ice–hydrate mixtures at negative temperatures were reported by E. Ershov, V. Istomin, Yu. Lebedenko, E. Chuvilin, and V. Yakushev in March 1988 at the geocryology session of the USSR Academy of Sciences and in October 1988 at the workshop on comparative planetology. Then, the ability of gas hydrates to preserve at below-equilibrium pressures was the subject of several publications [16–19]. However, works on hydrate dissociation and self-preservation in the pore space of frozen rocks, where gas hydrates are presented in the form of pore cement [20–29], are still much more scarce than the theoretical and experimental studies for the cases of unconfined gas hydrates [8,30–46].

In general, the dissociation of gas hydrates at below-equilibrium pressures and temperatures from 238 to 273 K begins with the decomposition of hydrate particles into liquid supercooled water and gas. As shown by thermodynamic calculations and laboratory experiments, supercooled water can remain on the surface of methane hydrate particles for a few h at <0 °C [37]. At the same time, the heat-consuming dissociation process cools down the system [15], whereby supercooled water freezes up and makes a growing ice film over hydrate particles, which slows down the dissociation. On the other hand, gas hydrates may partly convert to ice and back, and ice can undergo metamorphism in a zone of recrystallization at the ice–hydrate boundary [34,35,47]. At temperatures as low as <238–243 K, dissociation does not stop, as no unfrozen water can form [8,18].

The patterns of hydrate formation and dissociation in the pore space differ markedly from the respective unconfined processes. Furthermore, the available published evidence [18,48–62] shows that the presence of pore gas hydrates changes the thermal and mechanic properties of permafrost, as well as its permeability and behavior in response to chemistry and P-T changes. Experiments confirm that natural gas hydrates are vulnerable to external impacts and thus pose geological risks in the exploration and operation of Arctic oil and gas fields. Despite the great practical interest regarding intrapermafrost pore gas hydrates (mainly in sandy and silty soils), their dissociation and preservation remain poorly understood. We are trying to gain more insights from special laboratory experiments into the self-preservation of gas hydrates in frozen sediments.

2. Materials and Methods

The experiments were performed using two systems for laboratory hydrate saturation within user-specified temperature and pressure ranges. One system is a pressure cell of a ~420 cm^3 working volume that is designed as a tight steel cylinder and is 100 mm in diameter and 110 mm high, with holes for gas delivery and the connection of sensors and a steel lid tightened by a Teflon gasket. Soil samples are placed into a 100 mm high container of an inner diameter of 46 mm. Pressure is monitored by a digital pressure gage mounted on the lid top, and temperature is measured by thermistors attached to the samples via a plug in the cell bottom and through special holes on the side of the core holder. The temperature and pressure changes during the experiments are read automatically to an accuracy of 0.05 °C and 0.005 MPa. The acquired data are saved to a PC with a built-in ADC [20,63,64]. Gas is injected through holes in stamps on the sample top and bottom. The system is vacuumed using a low-power pump. Temperature is maintained with a Haake Phoenix C40P refrigerated circulator. The temperature-controlled liquid circulates around the pressure cell from the refrigerated bath along the "thermal coat".

The other system (Figure 1), manufactured by Top Industrie (Vaux-le-Pénil, France), is likewise a pressure cell (570 cm^3 volume; 70 mm inner diameter; 150 mm high), which can maintain a working pressure up to 15 MPa. The system is equipped with a JULABO liquid cryostat (Seelbach, Germany) that ensures operation in a temperature range from −20 °C to +40 °C. The system allows for the investigation of the formation and preservation of pore gas hydrates in frozen samples at different pressures and temperatures. The temperature and pressure are maintained at an accuracy of 0.1 °C and 0.1 MPa, respectively [64,65].

(a)   **(b)**
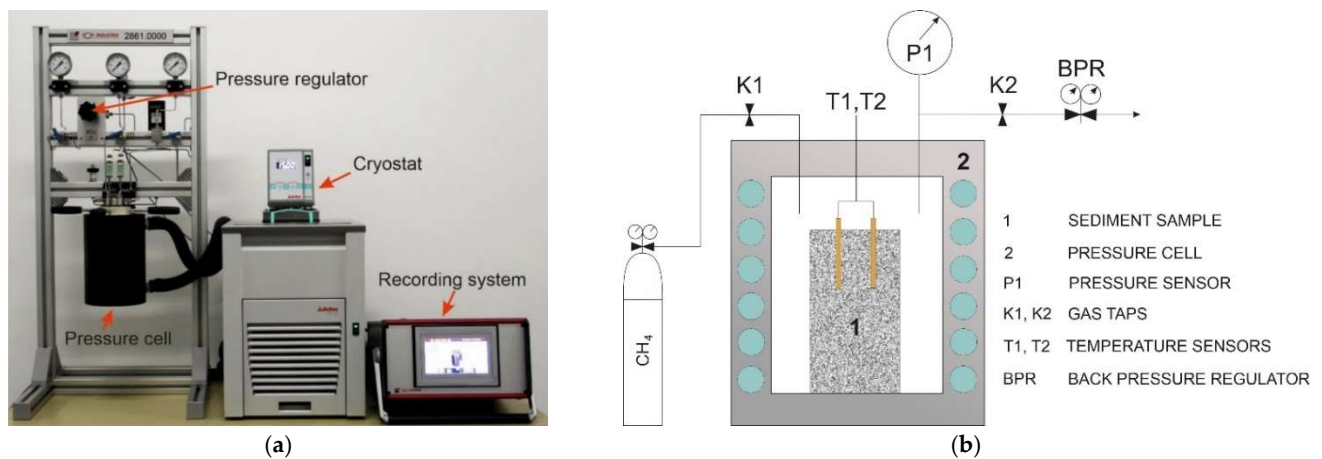
Figure 1. Top Industrie system for hydrate-saturated samples: general view (**a**) and a sketch of the pressure cell interior (**b**).

The pressure cell is a tight steel cylinder with a heat insulation jacket and tubes for the delivery of cooling liquid. The samples are placed into the pressure cell in a plastic container that is 100 mm high and 46 mm in diameter. The temperature is measured by two temperature sensors, which are 40 and 60 mm long and 1 mm in diameter, mounted on the cell lid together with fittings for gas injection and gas pressure measurement.

The experiments were applied to natural Early-Middle Pleistocene glacial genesis sand and Paleogene eluvial genesis clay silt samples (Tables 1 and 2).

Table 1. Lithology and mineralogy of samples.

Sample	Sampling Site	Mineralogy, %	
Sand 1	Lubertsy	Quartz	>90
Sand 2	Yamburg GCF	Quartz	38
		Microcline+Albite	45
		Illite	9
		Kaolinite + Chlorite	5
Sand 3	South-Tambey GCF	Quartz	>93
Montmorillonite clay	Dzhembel (Turkmenistan)	Montmorillonite	93.4
		Andesine	2.9
		Biotite	2.9
Kaolinite clay	Novokaolinovy (Chelyabinsk region)	Kaolinite	92
		Quartz	6
		Muscovite	2

Note: GCF = gas condensate field.

Table 2. Properties of samples.

Sample	Particle Size Distribution, %			Salinity, %	Solid Particles Density, g/cm^3	Classification *
	1–0.05 mm	0.05–0.001 mm	<0.001 mm			
Sand 1	100	—	—	0.01	2.65	Fine sand
Sand 2	84.3	13.7	2	0.09	2.60	Fine sand
Sand 3	95.6	4.4	—	0.08	2.60	Fine sand
Montmorillonite clay	0.3	46.2	53.5	1.99	2.45	Heavy clay
Kaolinite clay	4.5	70.9	24.6	0.04	2.66	Silty clay

Note: * Classification is given according to [66].

The samples were saturated with water to specified initial moisture contents and with pure methane (99.98% CH$_4$) as a hydrate-forming gas. To achieve the wanted moisture content, sand was oven-dried at 105 °C for 8 h, sieved through 1 mm mesh, mixed with

distilled water, and left for 30 min at room temperature. Then, the wet soil was compacted layer-by-layer in a cylindrical container (Figure 2) and placed into the pressure cell. The pressure cell with the samples was tightly sealed, vacuumed, and filled with hydrate-forming gas (methane) [26,64].

Figure 2. General view of the frozen sand 3 sample with pore methane hydrate (W = 14%; S_h = 26%; T = −6 °C).

Hydrate saturation started at negative temperatures of −5 °C to −6 °C and pressures of 4–8 MPa. After the injection of cooled methane, the temperature in the pressure cell with the frozen samples was maintained at constant negative values for a few days in order to avoid moisture re-distribution during hydrate formation. Then, the samples were exposed to several freezing–thawing cycles to increase hydrate contents, and the temperature of the system gradually rose to low positive values of +1 to +3 °C. As the ice was melting, pore hydrate formation accelerated due to additional gas–water contacts associated with residual pore water that did not convert to hydrate before [64]. Once the hydrate formation in the frozen samples (−5 to −6 °C) had completed, the pressure in the cell was reduced to the below-equilibrium level of 0.1–1.7 MPa, which triggered hydrate dissociation. This approach allowed for the study of the dissociation kinetics at the P-T conditions close to pressures and temperatures in the gas reservoir depth interval.

The phase transition parameters and hydrate formation features can be inferred from pressure and temperature variations in the test cell. The hydrate saturation (S_h), ice saturation (S_i), hydrate coefficient (K_h), and self-preservation coefficient (K_{sp}) of metastable gas hydrates were found using the pressure–volume–temperature (PVT) analysis [26,64,67].

Hydrate saturation (S_h, %), which is the percentage of pore space filled with hydrate, is found from the volume content of hydrate H_v (%) and porosity n (u.f.):

$$S_h = \frac{H_v}{n} \tag{1}$$

The hydrate coefficient (K_h, u.f.), which is the fraction of water converted to hydrate, is given by

$$K_h = \frac{W_h}{W} \tag{2}$$

where W_h is the percentage of water converted to hydrate (% of dry sample weight) and W is the total initial amount of moisture (%). W_h is found from the weight of pore hydrate M_h, which is calculated using gas absorption, with reference to the methane hydrate formula $CH_4 \cdot 5.9H_2O$.

The self-preservation coefficient (K_{sp}), which is a ratio of the hydrate saturation in the end of the run to the initial value, is found as

$$K_{sp} = \frac{H_v^{st}}{H_v^{in}} \tag{3}$$

where H_v^{in} is the initial volume content of hydrate at equilibrium conditions and H_v^{st} is the final value at below-equilibrium pressure.

After the hydrate formation had completed, the cell with the frozen samples (−6 to −7 °C) was opened, and the samples were taken out, photographed, and analyzed in terms of physical properties: structure and texture, moisture content, gas hydrate contents, etc.

In some runs, gas contents in the samples were determined after the pressure in the cell dropped to 0.1 MPa in order to quantify the percentage of pore gas hydrate. The gas contents were estimated as in [20]. The samples of frozen hydrate-bearing soil were weighed and placed in a ~20% NaCl solution at room temperature under a gas collecting tube. The volume of released gas was inferred from the level changes of the liquid, and the frozen hydrate-bearing samples covered with crushed ice to prevent sublimation were placed in boxes for prolonged storage at negative temperatures. The time-dependent changes in gas and hydrate contents until the dissociation process stopped were recorded in specimens selected from those samples.

The dissociation of gas hydrates in thawing samples leads to methane emission. The amount of emitted gas was estimated from the calculated hydrate saturation (S_h), weight (H) and volume (H_v) hydrate contents, and physical properties of the samples (volume V, weight m, and density ρ). The amount of released methane after the pressure drop was calculated as a bulk value and per cubic meter of the hydrate-bearing rock.

The amount of residual unfrozen pore water in frozen sediments containing self-preserved pore hydrates at below-equilibrium pressures was estimated using the nuclear magnetic resonance (NMR) technique on an Oxford Instruments Geospec 2-53 Benchtop NMR Rock Core Analyzer (Figure 3).

(**a**)　　　　　　　　　　　　　　　　　　　　(**b**)

(**c**)
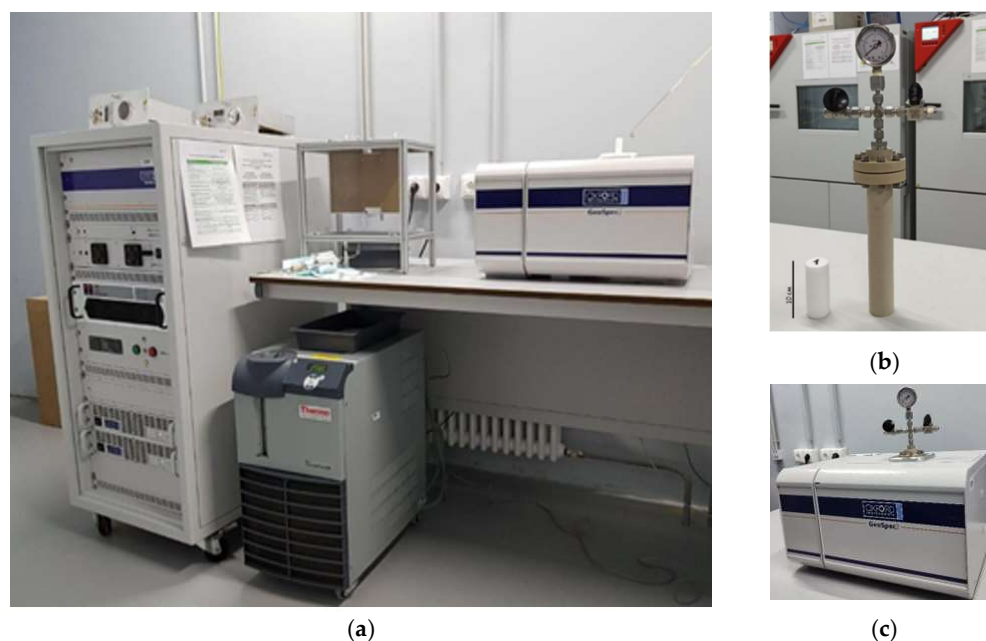
Figure 3. Oxford Instruments Geospec 2-53 Benchtop NMR Rock Core Analyzer (general view) (**a**); high-pressure core holder (**b**); core holder mounted on the NMR cell (**c**).

The NMR method, which is currently of broad use for studies of gas hydrates and hydrate-bearing porous media [68–71], works as follows. Permanent magnets of a nuclear magnetic relaxometer create a uniform magnetic field which acts on the hydrogen nuclei and aligns their chaotic magnetic moments with the main field. Hydrate-bearing soil samples are placed into the uniform magnetic field and are exposed to the Carr–Purcell-Meiboom–Gill (CPMG) pulse sequence. The CPMG pulses produce a closely spaced train of spin echoes whose decay is analyzed to determine the time of transverse relaxation T_2 (ms). Then, the total volume of liquid pore water (cm^3) is calculated from processed magnetization decay and T_2 values and is then recalculated into wt% with regard to soil

properties. The data are processed using the GIT Systems Advanced v.7.5.1 software (Green Imaging Technologies).

The Geospec 2-53 NMR analyzer is operated at a frequency of 2.28 MHz, with a magnetic field of 0.05 T, and includes an additional set of gradient coils mounted along the magnet. It allows for the estimation of the total volume of the liquid phase in the samples and yields its 1D profile along the sample height. The better accuracy of measurements is achieved by calibration against a reference sample with a precisely measured volume of the liquid phase (4.7 mL, with 10 % NaCl).

The experiments were run using a core holder specially designed for measuring the amount of liquid pore water in hydrate-bearing samples under different gas pressures. The core holder is a pressure cell with an inner diameter of 20 mm and a working volume of ≈40 cm^3, equipped with a gas pressure gauge, seamless tubes, and fittings for gas delivery. It is mainly made of a durable plastic material (polyether ether ketone PEEK Zedex-324), except for a few elements on the top which are not placed into the NMR cell (Figure 3b). The material can tolerate temperatures from −60 °C to +250 °C and has low thermal conductivity (~0.2 W/m·K) and specific heat (~1.0 kJ/kg·K), has a high tensile strength (40 MPa) comparable to that of stainless steel, and does not contribute much noise to the data. The pressure cell was tested at 16 MPa, but the working pressure was limited to 8 MPa for safety reasons; the temperature was set between −10 °C and +25 °C.

3. Results and Discussion

The dissociation of pore gas hydrates in frozen sediments is known from the available published data to differ from the respective process in unconfined conditions. The size, shape, and structure of hydrate inclusions depend largely on the texture, ice and hydrate saturation, and hydrate formation patterns in their host sediments.

Pore ice in hydrate-bearing frozen sediments only partly converts to hydrate, while the remaining ice affects the preservation of pore gas hydrates, which become metastable upon the pressure dropping below equilibrium. Residual ice actually provides primary stabilization until the partial hydrate dissociation produces secondary ice.

The dissociation kinetics of pore methane hydrate are recorded as time-dependent changes in ice (S_i) and hydrate (S_h) saturation (Figure 4). Prior to the pressure drop, 46% of the pore space was filled with hydrate, while the ice saturation was 3%. The S_h curve after the pressure drop to 0.1 MPa comprises three segments of rapid (1), slower (2), and very slow (3) dissociation (Figure 4). After the abrupt hydrate saturation decrease, the water released by dissociation converted to ice, and the ice saturation increased correspondingly. For the first 100 hr of rapid hydrate dissociation, S_h reduced to 20%, while S_i increased to 35%. At the end of the process, the respective values were 10.2% and 44% (Figure 4).
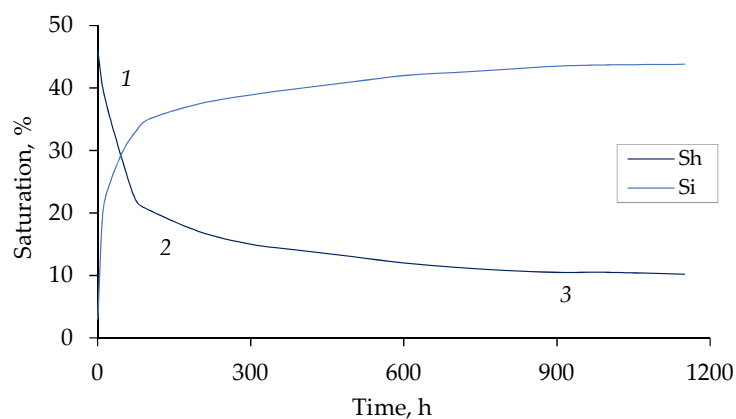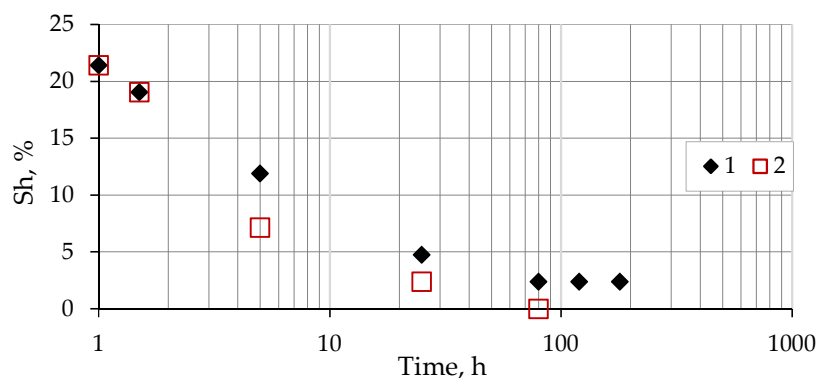

Figure 4. Time-dependent changes in methane hydrate (S_h) and ice (S_i) saturation in the sand 2 sample (W = 20%) at T = −6.5 °C after the pressure dropped to 0.1 MPa.

In addition to pressure and temperature, the dissociation kinetics and preservation of pore gas hydrates are controlled by the grain size, mineralogy, texture, salinity, and initial ice saturation of sediments, as well as by the structure distortion in hydrate particles. The effects of these factors were studied in separate experiments.

3.1. Structure Defects in Gas Hydrate Particles

The dissociation and self-preservation of pore gas hydrates at the given pressure and temperature conditions depend on the size of hydrate inclusions and the distortion of their structure: dissociation becomes faster while self-preservation reduces in deformed gas hydrates with cracks and structural defects. The effect of deformation on the stability of self-preserved pore gas hydrates can be estimated in frozen sediments exposed to cyclic temperature changes. Pore methane hydrates in samples cooled down from −7 °C to −50 °C (at 0.1 MPa) by soaking in liquid nitrogen for one or two h dissociated faster than those from samples stored at a constant negative temperature (Figures 5 and 6). Hydrate saturation in sand 1 containing 3% of montmorillonite clay reduced to 1% in 24 h and became undetectable in 77 h. However, the hydrate saturation of a similar sample not exposed to cooling in liquid nitrogen decreased slowly to 2.4% after 77 h and then remained invariable for 180 h (Figure 5).

Figure 5. Time-dependent changes in the methane hydrate (S_h) saturation of sand 1 with 3% of montmorillonite clay (W = 10%) after the pressure dropped to 0.1 MPa: not cooled (1) and cooled (2) in liquid N$_2$.
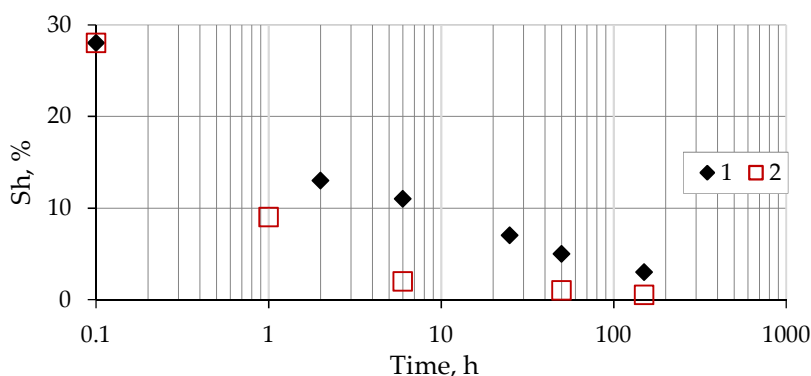
Figure 6. Time-dependent changes in the methane hydrate (S_h) saturation of sand 1 with 14% of kaolinite clay (W = 14%) after the pressure dropped to 0.1 MPa: not cooled (1) and cooled (2) in liquid N$_2$.

The sand 1 sample with 14% of kaolinite clay showed a similar behavior upon cooling in liquid nitrogen: its hydrate saturation reduced to 1% in 50 h and was almost zero in 93 h after the recovery from liquid nitrogen, while the respective S_h value in the absence of cooling was ~3% (Figure 6).

This behavior of pore gas hydrates is apparently due to the deformation caused by cooling: the dissociation accelerated in the presence of microcracks [72] that formed in response to the relaxation of cooling-related stress [73].

### 3.2. Clay Content and Mineralogy

The behavior of pore gas hydrates in frozen sediments also depends on the percentage and composition of the clay component. Clay particles added to sand increase its specific surface area and the contents of bound unfrozen water. The effect of clay mineralogy is especially evident in the case of montmorillonite and kaolinite clay. Montmorillonite clay, which displays lattice expansion when exposed to water, has a higher specific surface activity and contents of bound water than kaolinite clay.

The sensitivity of pore hydrate dissociation to the mineralogy of the clay component in frozen sand was studied using a sand–clay mixture (a clay content up to 14% and an initial water content of about 10%) under below-equilibrium pressure (0.1 MPa) and a negative temperature of −6.5 °C. Thirty minutes after the pressure drop to 0.1 MPa, the accumulation of pore methane hydrate in samples with 7% of montmorillonite clay decelerated: the hydrate coefficient decreased from 0.75 to 0.36 u.f. (Table 3).

Table 3. Hydrate coefficient in frozen sand with montmorillonitic clay under equilibrium and below-equilibrium (0.1 MPa) pressures, t = −6.5 °C.

Sample	Clay Content, % (Montmorillonite)	Hydrate Coefficient		K_h Reduction, %
		Equilibrium Pressure	30 min After Pressure Drop to 0.1 MPa	
		K_h Initial, u.f.	K_h, u.f	
1	0	0.75	0.72	3.6
2	3	0.40	0.37	7.5
3	7	0.36	0.29	19

The dissociation of pore methane hydrate was faster in sand samples with montmorillonite clay than it was in those with kaolin at the same clay content of 14% (Figure 7): the hydrate saturation five h after the pressure drop was 20 % against 10%, respectively.
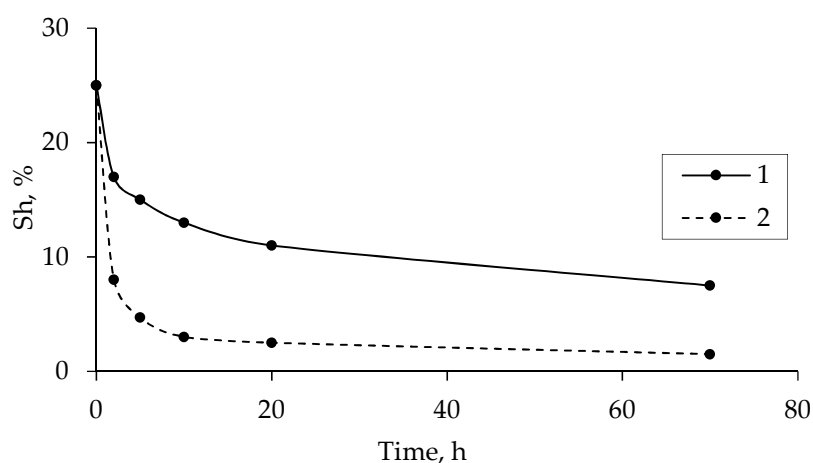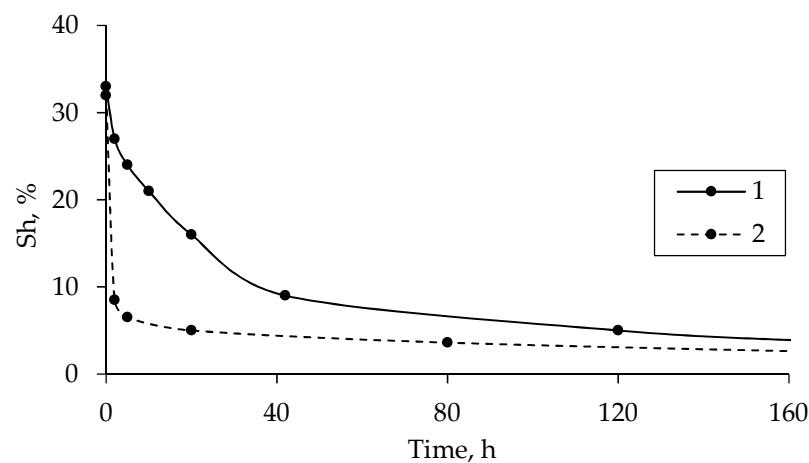

Figure 7. Time-dependent changes in the methane hydrate saturation (S_h) of frozen sand 1 with 14% of kaolinite (1) and montmorillonite (2) clay (W = 14%) after the pressure dropped to 0.1 MPa at −6.5 °C. Black dots are experimental data; the solid line is a trend line of exponential approximation.

Ten h after the pressure drop, the dissociation rates in the two samples became almost equally slow due to the self-preservation effect. Seventy h after the onset of dissociation, the hydrate saturation (S_h) values in the samples with kaolinite and montmorillonite clay

were, respectively, ~8% and 1.5%. The difference is due to higher contents of unfrozen pore water and lower ice contents in the latter case, which creates unfavorable conditions for the self-preservation of the pore gas hydrate.

On the other hand, frozen (−6.5 °C) sand containing 7% of kaolinite particles showed much faster hydrate dissociation upon the pressure dropping than pure sand (Figure 8), even though the two samples had similar initial hydrate saturation percentages (33 and 34%). Thirty min after the pressure drop, the saturation decreased by no more than 4% in pure sand but became almost four times lower in the sample with kaolinite clay. Further on, the dissociation rate decayed quite rapidly in the sand + clay sample but continued even after 80 h in the pure sand. The reason may be that hydrate dissociation led to the rapid cooling of the clay-bearing sample at the beginning of the run. At the end of the run (160 h), the hydrate saturation values in pure sand and in sand with 7% kaolin were, respectively, 4.3% and 2.5%.

Figure 8. Time-dependent changes in the methane hydrate (S_h) saturation of pure sand 1 (1) and sand 1 with 7% of kaolinite clay (2) (W = 10%) after the pressure dropped to 0.1 MPa at −6.5 °C. Black dots are experimental data; the solid line is a trend line of exponential approximation.

The rapid dissociation of pore methane hydrates in sand with higher clay contents is due to the higher amounts of unfrozen pore water, which interferes with the self-preservation process, as well as due to the morphology of hydrate inclusions. Pore gas hydrates in finer sediments occur as hydrate caps and thus have higher total contents and dissociate more slowly.

3.3. Hydrate Saturation

The preservation of pore gas hydrates in frozen sediments exposed to below-equilibrium pressure (0.1 MPa) is sensitive to saturation with ice and gas hydrate. The saturation effect was studied in samples of frozen sand 1 with initial moisture contents of 5% and 10% and with hydrate saturations of 22% and 34%, respectively. During the first hour after the pressure drop to 0.1 MPa, pore methane hydrates dissociated 2.5 times faster in the drier sample (W = 5%) than in that with W = 10 % (Figure 9).

After 20 h of dissociation, the hydrate saturation decrease was more than two-fold in the sample with W = 5% but was within 25% in the wetter sample. Then, the dissociation decayed as ice formed on the surfaces of hydrate particles. After 40 h of the process, hydrate saturation stabilized at 8% in the wetter sample and approached zero in the drier one.

The experiments showed that the ice films, which formed by the freezing of residual moisture not converted to hydrate, increased the stability of pore gas hydrates. Their dissociation decayed faster until the complete hydrate stabilization in sediments with higher ice contents.
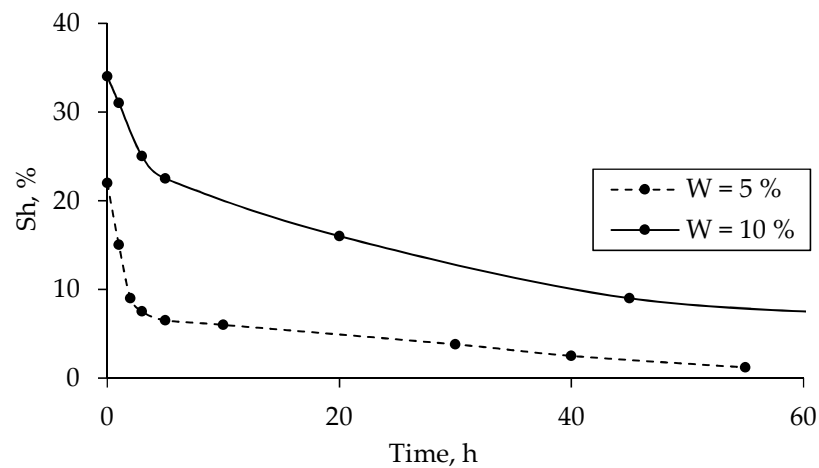
Figure 9. Time-dependent hydrate saturation in sand 1 samples with initial moisture contents of 5% and 10% after the pressure dropped to 0.1 MPa at −6 °C. Black dots are experimental data; the solid line is a trend line of exponential approximation.

3.4. Salinity

The dissociation of pore gas hydrates in frozen sediments exposed to below-equilibrium pressure (0.1 MPa) is largely sensitive to salinity. The presence of dissolved salts affects the phase composition of pore moisture and the amount of residual liquid water: the ice coats around hydrate crystals form more slowly and become less dense as the amount of liquid water increases, which reduces the stability of pore methane hydrate at pressures below equilibrium. The effect of salinity on the dissociation kinetics of pore methane hydrates was studied in samples of nonsaline (0.01%) and saline (0.2%) sand 1 with W = 10%. The initial hydrate saturation in the nonsaline and saline samples was 35% and 31%, respectively. Pore gas hydrates in saline sand dissociated rapidly and reached zero saturation two h after the pressure drop to 0.1 MPa, while the hydrate saturation of the nonsaline sample only reduced to 8% (Figure 10).
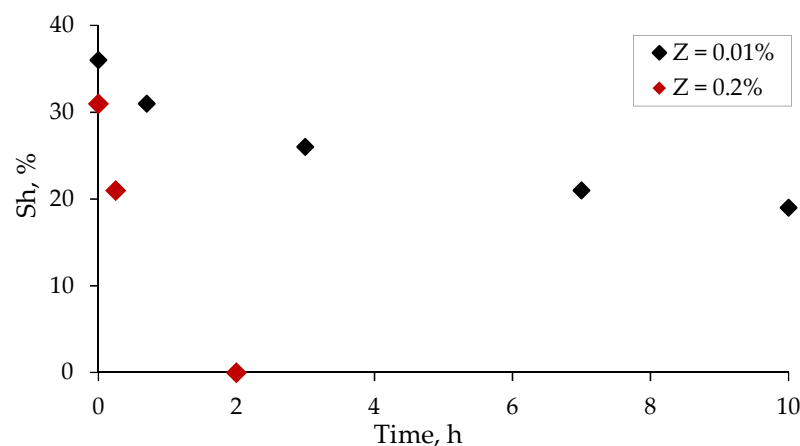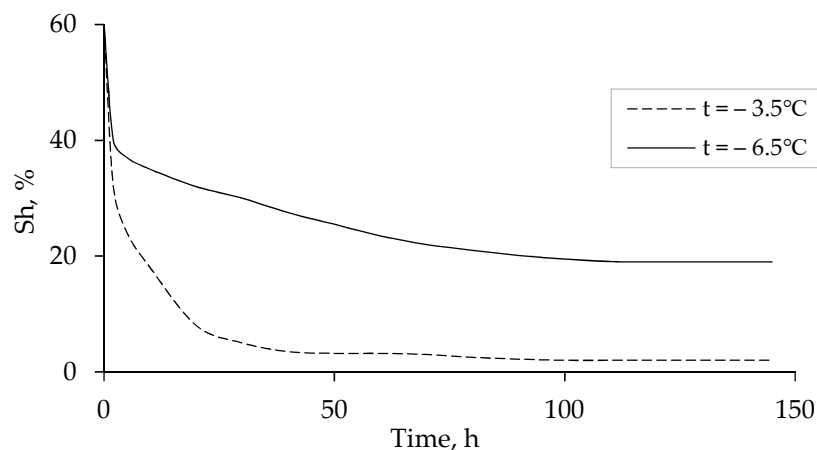

Figure 10. Time-dependent hydrate saturation in saline (Z = 0.2%) and nonsaline (Z = 0.01%) sand 1 samples (W = 10%) after the pressure dropped to 0.1 MPa at −6 °C.

3.5. Temperature

Temperature strongly influences the preservation of metastable pore gas hydrates in permafrost [26]. According to experimental evidence, hydrate dissociation in response to pressure drops decelerates markedly at temperatures below −4 °C. The dissociation of pore methane hydrate in sand 2 samples, with W = 18% and S_h = 60%, showed different kinetics at −3.5 °C and −6.5 °C (Figure 11). It was rapid at a higher temperature (−3.5 °C): hydrate saturation reached 8% after 20 h and 2% after 100 h. The respective saturation

values at −6.5 °C were 32% and −20%, and the latter value remained almost invariable until the run ended (Figure 11). In general, cooling impedes dissociation and increases the percentage of self-preserved gas hydrates.

Figure 11. Time-dependent hydrate saturation in the frozen sand 2 sample (W = 18%) after the pressure dropped to 0.1 MPa at −3.5 °C and −6.5 °C.

However, pore gas hydrates dissociate especially rapidly at temperatures beyond the self-preservation range (50 °C). The hydrate saturation of frozen sand 1 containing 7% of montmorillonite clay (W = 17%) was two times lower at −50 °C than it was at −7 °C twenty-two h after the pressure dropped (Figure 12), and the difference became four-fold by the end of the run (50 h). After 72 h, pore methane hydrate was undetectable in the samples cooled to −50 °C, but hydrate saturation remained stable (at ~12%) in the case of −7 °C.
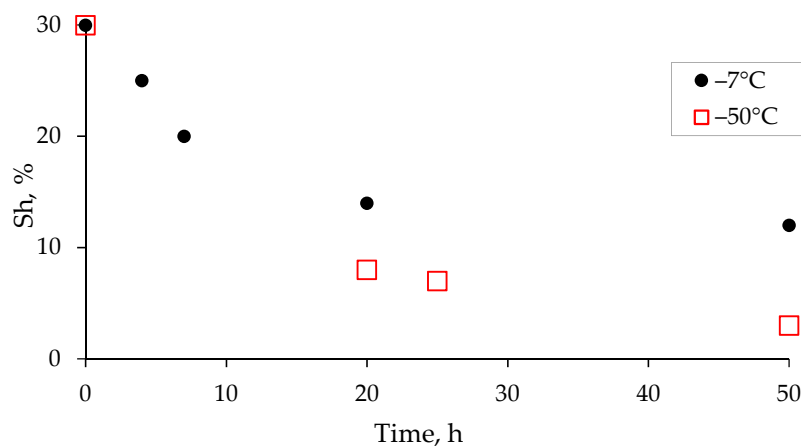
Figure 12. Time-dependent hydrate saturation in the frozen sand 1 sample with 7% of montmorillonite (W = 17%) after the pressure dropped to 0.1 MPa at −7 °C and −50 °C.

The lower stability of the pore methane hydrate in frozen rocks at −50 °C is consistent with previous data [17] for hydrate dissociation below the temperatures of the self-preservation range.

3.6. Gas Pressure

With the negative temperature being constant, non-equilibrium gas pressure is another important control of pore gas hydrate dissociation and self-preservation in frozen sediments. Pressure increases during pore hydrate dissociation make the process slower or even lead it to a complete stop as they bring the system to a new equilibrium.

The effect of gas pressure on the hydrate dissociation kinetics was tested on sand 3 samples with 60% initial methane hydrate saturation (Figure 13) at pressures of 0.1, 1.3,

and 1.7 MPa. Dissociation stopped four h after the pressure drop to 1.7 MPa but continued for the whole run (24 h), decelerating gradually in the cases of lower pressures.
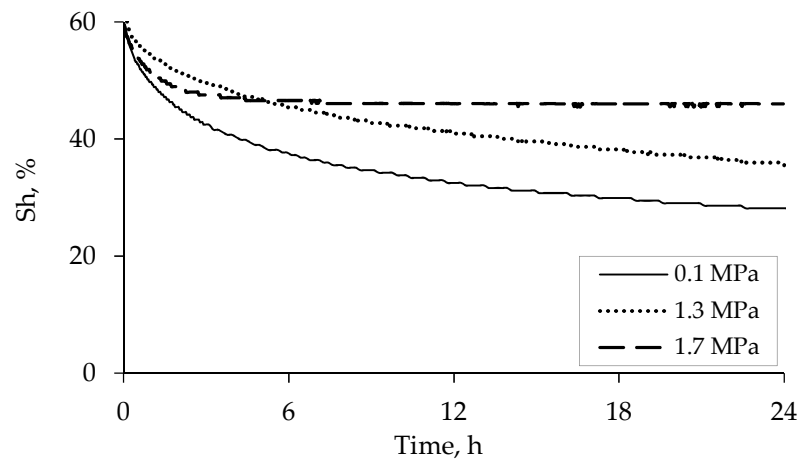
Figure 13. Time-dependent hydrate saturation in frozen sand 3 samples after the pressure dropped to 0.1, 1.3, and 1.7 MPa at −6 °C.

The dissociation stopped in the case of 1.7 MPa because the gas pressure in the system reached the equilibrium level for methane hydrate. In the two other cases, the hydrate saturation 24 h after the run onset was about 36% at 1.3 MPa and within 28% at 0.1 MPa.

Thus, pore gas hydrates were confirmed experimentally to dissociate more slowly and remain better preserved at higher below-equilibrium pressures.

The reported experimental and theoretical results, as well as the published evidence, show that the dissociation and self-preservation of pore gas hydrates in frozen sediments exposed to below-equilibrium pressures are sensitive to the amount of residual unfrozen pore water and its variation in time. At higher contents of unfrozen water due to external (pressure and temperature) or internal (salinity, clay content, and mineralogy) factors, self-preservation becomes less efficient. A decrease in the temperature of frozen hydrate-bearing sediments in the area of self-preservation (−2 °C to −35 °C) contributes to an increase in the preservation of pore hydrate. Rapid and/or deep cooling reduces the self-preservation ability of pore gas hydrates as it leads to thermal strain and stress with the formation of microcracks and other structural defects of the ice–hydrate component. This inference has been corroborated by experiments on frozen hydrate-bearing sediments soaked in liquid nitrogen, either briefly or for prolonged storage.

On the other hand, dissociation at lower equilibrium pressures produces additional amounts of supercooled liquid pore water in frozen hydrate-bearing sediments, which freezes up with time at negative temperatures. The lifespan of this water largely influences the self-preservation efficiency of gas hydrates.

As follows from our NMR data for frozen hydrate-bearing sand 1 (W = 6.0%), considerable amounts of liquid pore water may form early during hydrate dissociation in response to the pressure dropping below the equilibrium (Figure 14). The time-dependent behavior of liquid water contents correlates with the dissociation kinetics. For the first 40 min after the pressure drop from 5.0 MPa (equilibrium) to 0.1 MPa at −5.5 °C, when hydrate dissociation was especially rapid, the amount of unfrozen pore water increased from 0.1 wt% to 0.9 wt%. It held at this level in the following 24 h and increased to 1.0 wt% (possibly higher in the first few hours of rapid dissociation), while the dissociation rate decreased slightly.
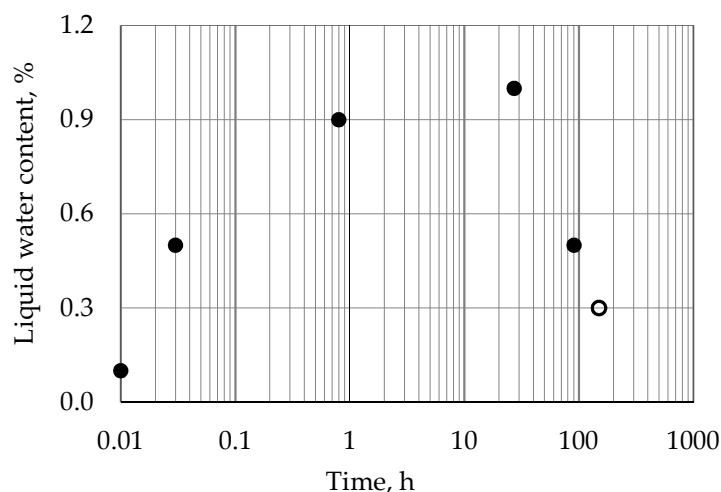
Figure 14. Time-dependent changes in liquid pore water contents in frozen hydrate-bearing fine sand 1 (W = 6.0 %; K_h = 98%) after the pressure dropped to 0.1 MPa at −5.5 °C. Bold circles are experimental data (this study); open circles are the previous data of Chuvilin et al., 2022 [74].

However, the dissociation process decays as the supercooled pore water freezes up and forms an ice film on the surface of hydrate particles. The unfrozen water contents decrease correspondingly: ninety h after the pressure drop, the sand sample contained 0.5 wt% of liquid water. The decrease can be expected to continue until the equilibrium value (~0.3 wt%) for the given soil type at the given temperature (−5.5 °C) [74].

Thus, the NMR results show that supercooled unfrozen pore water in frozen hydrate-bearing sediments can hold for several days during the dissociation of pore gas hydrates upon the pressure decreasing below the equilibrium. Similar inferences regarding the possible lifespan of residual liquid water during the dissociation of gas hydrates at temperatures below 0 °C were suggested previously [75–77], but only for bulk conditions and for the period of a few hours after the pressure drop. Our experimental results extend the existing ideas on the mechanisms of pore gas hydrate self-preservation in permafrost [8].

The experimentally observed self-preservation patterns of pore gas hydrates depend on the properties and composition of the host frozen sediments, as well as on the pressure and temperature conditions. The revealed sensitivity of hydrate dissociation kinetics to clay contents and mineralogy, salinity, ice contents, temperature, and gas pressure has a bearing on the role of these factors in the self-preservation of pore gas hydrates. Thus, the conditions for the better preservation of metastable pore hydrates in permafrost [26] can be constrained proceeding from the patterns of ice film formation around hydrate particles at below-equilibrium pressures. The conditions and processes that produce cracks and defects in the ice film and attenuate its thickness, as well as decelerate the freezing of unfrozen pore water (e.g., if its amount is large enough), are expected to interfere with hydrate self-preservation.

Predicting the contents of relict metastable pore gas hydrates in permafrost requires data on past conditions for hydrate accumulation and preservation at non-equilibrium pressures. According to the experiments, the hydrate saturation of permafrost at metastable conditions can reach ~20% (and sometimes more). The warming and thawing of permafrost that contains metastable pore gas hydrates can lead to methane emission depending on residual hydrate saturation. For instance, the residual hydrate saturation of frozen sand 3 exposed to prolonged conditions of self-preservation at −6 °C varied from 13 to 26%. The methane emission from such sediments in the case of their thawing can reach 16 m^3 per 1 m^3 of hydrate-bearing permafrost (Figure 15).
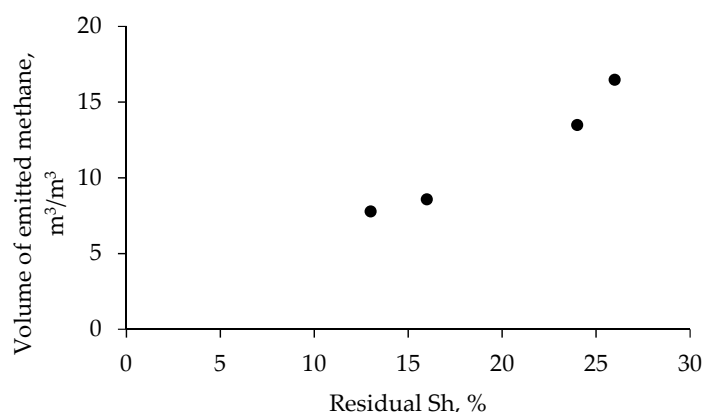
Figure 15. Methane emission upon the temperature increase in frozen hydrate-bearing sand 3 as a function of residual hydrate saturation.

4. Conclusions

The available published materials and our experimental results show that the dissociation and self-preservation patterns of pore gas hydrates at negative temperatures differ from the respective processes in bulk conditions and depend on temperature, pressure, the morphology of hydrate inclusions, and the properties of the host sediment (including texture and structure).

The contents of relict (metastable) gas hydrates in permafrost can be inferred from data on past hydrate accumulation conditions, as well as on conditions for their preservation at non-equilibrium pressures.

Pore gas hydrates were shown experimentally to dissociate more rapidly and to be worse preserved in warming saline sediments with higher clay contents and lower hydrate and ice saturations. Pore gas hydrates are better preserved within the temperatures that can maintain their self-preservation than they are at lower negative temperatures (outside this range). Low-temperature impacts on frozen hydrate-bearing sediments lead to a decrease in the safety of metastable porous gas hydrates.

The self-preservation of pore gas hydrates at below-equilibrium pressures is highly sensitive to the amount of residual unfrozen pore water and its variations in time. According to the NMR data, supercooled water can hold for a few days in the pores of frozen soil, while pore gas hydrates are dissociating in response to the pressure dropping below the equilibrium.

According to the evidence of laboratory experiments and calculations, the methane emissions from warming permafrost containing metastable pore gas hydrates can reach 16 m^3 or more per 1 m^3 of frozen soil. Methane emissions can pose risks to engineering facilities in permafrost, especially for producing oil and gas wells in the Arctic regions.

Author Contributions: Conceptualization, experimental methodology, supervision, E.C.; calculation methodology, E.C. and V.I.; experiments, processing, analysis, E.C., D.D. and B.B.; NMR experiments, A.M. and B.B.; writing—original draft, E.C., D.D.; writing—review and editing, E.C., D.D., B.B. and A.M. All authors have read and agreed to the published version of the manuscript.

Institutional Review Board Statement: Not applicable.

Informed Consent Statement: Not applicable.

Data Availability Statement: Not applicable.

Conflicts of Interest: The authors declare no conflict of interest.

References

1. Chersky, N.J.; Makogon, Y.F. Solid Gas World Reserves Are Enormous. *Oil Gas Int.* **1970**, *10*, 82–84.
2. Max, M.D. *Natural Gas Hydrate in Oceanic and Permafrost Environments*; Kluwer Acad: Dordrecht, London, UK, 2000; p. 414. ISBN 1384-6434. [CrossRef]
3. Sloan, E.D.; Koh, C.A. *Clathrate Hydrates of Natural Gases*, 3rd ed.; CRC Press: Boca Raton, FL, USA, 2008; p. 752. ISBN 9780429129148. [CrossRef]
4. Dallimore, S.R.; Collett, T.S. Interpermafrost gas hydrates from a deep core hole in the Mackenzie Delta, Northwest Territories, Canada. *Geology* **1995**, *23*, 527–530. [CrossRef]
5. Dallimore, S.R.; Chuvilin, E.M.; Yakushev, V.S.; Grechischev, S.E.; Ponomarev, V.; Pavlov, A. Field and laboratory characterization of interpermafrost gas hydrates, Mackenzie Delta, NWT Canada. In Proceedings of the 2th International Conference on Gas Hydrate, Toulouse, France, 2–6 June 1996; pp. 525–531.
6. Chuvilin, E.M.; Yakushev, V.S. Structure and some properties of frozen hydrate-containing soils. In Proceedings of the International Symposium on Methane Hydrates Resourses in the Near Future, JNOC, Chiba City, Japan, 20–22 October 1998; pp. 239–246.
7. Yakushev, V.S.; Chuvilin, E.M. Natural gas and hydrate accumulation within permafrost in Russia. *Cold Reg. Sci. Technol.* **2000**, *149*, 46–50. [CrossRef]
8. Istomin, V.A.; Yakushev, V.S.; Mokhonina, N.A.; Kwon, V.G.; Chuvilin, E.M. Self-preservation phenomenon of gas hydrate. *Gas Ind. Russ.* **2006**, *4*, 16–27. (In Russian)
9. Davidson, D.W.; Garg, S.K.; Gough, S.R.; Hand, Y.P.; Ratcliffe, C.I.; Ripmeester, J.A.; Tse, J.S.; Lawson, W.F. Laboratory analysis of a naturally occurring gas hydrate from sediment of the Gulf of Mexico. *Geochim. Cosmochim. Acta* **1986**, *50*, 619–623. [CrossRef]
10. Handa, Y.P. Calorimetric determinations of the composition, enthalpies of dissociation and heat capacities in the range 85 to 270 K for clathrate hydrates of xenon and krypton. *J. Chem. Thermodyn.* **1986**, *18*, 891–902. [CrossRef]
11. Handa, Y.P. A calorimetric study of naturally occurring gas hydrates. *Ind. Eng. Chem. Res.* **1988**, *27*, 872–874. [CrossRef]
12. Yakushev, V.S. Experimental study of the methane hydrate dissociation kinetics at negative temperatures. *EI VNIIGazprom Ser. Dev. Oper. Gas Gas Condens. Fields* **1988**, *4*, 11–14. (In Russian).
13. Ershov, E.D.; Lebedenko, Y.P.; Chuvilin, E.M.; Yakushev, V.S. Experimental study of the microstructure of the ice-methane hydrate agglomerate. *Eng. Geol.* **1990**, *3*, 38–44. (In Russian).
14. Ershov, E.D.; Lebedenko, Y.P.; Chuvilin, E.M.; Istomin, V.A.; Yakushev, V.S. Features of gas hydrate occurrence in permafrost. *USSR Acad. Sci.* **1991**, *321*, 788–791. (In Russian).
15. Ershov, E.D.; Yakushev, V.S. Experimental research on gas hydrate decomposition in frozen rocks. *Cold Reg. Sci. Technol.* **1992**, *20*, 147–156. [CrossRef]
16. Gudmundsson, J.S.; Parlaktuna, M.; Knokhar, A. Storing natural gas as frozen hydrate. *SPE Prod. Facil.* **1994**, *9*, 69–73. [CrossRef]
17. Stern, L.; Circone, S.; Kirby, S.; Durham, W. Anomalous Preservation of Pure Methane hydrate at 1 atm. *J. Phys. Chem. B* **2001**, *105*, 1756–1762. [CrossRef]
18. Stern, L.; Circone, S.; Kirby, S.H.; Durham, W. Temperature, pressure, and compositional effects on anomalous or "self" preservation of gas hydrates. *Can. J. Phys.* **2003**, *81*, 271–283. [CrossRef]
19. Majid, A.A.A.; Koh, C.A. Self-Preservation Phenomenon in Gas Hydrates and its Application for Energy Storage. In *Intra- and Intermolecular Interactions between Non-Covalently Bonded Species*; Elsevier: Amsterdam, The Netherlands, 2021; pp. 267–285. [CrossRef]
20. Chuvilin, E.M.; Kozlova, E.V. Experimental estimation of hydrate-bearing sediments stability. In Proceedings of the 5th International Conference on Gas Hydrate Thermodynamic Aspects, Trondheim, Norway, 13–16 June 2005.
21. Chuvilin, E.M.; Guryeva, O.M. Experimental study of self-preservation effect of gas hydrates in frozen sediments. In Proceedings of the 9th International Conference on Permafrost, Fairbanks, AK, USA, 23 June–3 July 2008; pp. 263–267.
22. Kwon, T.-H.; Cho, G.-C.; Santamarin, J.C. Gas hydrate dissociation in sediments: Pressure-temperature evolution. *Geochem. Geophys. Geosyst* **2008**, *9*, Q03019. [CrossRef]
23. Chuvilin, E.M.; Buhanov, B.A.; Guryeva, O.M.; Istomin, V.A.; Takeya, S.; Hachikubo, A. Experimental study of self-preservation mechanisms during gas hydrate decomposition in frozen sediments. In Proceedings of the 7th International Conference on Gas Hydrates (ICGH 2011), Edinburgh, UK, 17–21 July 2011; pp. 1–9.
24. Hachikubo, A.; Takeya, S.; Chuvilin, E.; Istomin, V. Preservation phenomena of methane hydrate in pore spaces. *Phys. Chem. Chem. Phys.* **2011**, *13*, 17449–17452. [CrossRef] [PubMed]
25. Takeya, S.; Fujihisa, H.; Gotoh, Y.; Istomin, V.; Chuvilin, E.; Sakagami, H.; Hachikubo, A. Methane clathrate hydrates formed within hydrophilic and hydrophobic porous media: Kinetics of dissociation and distortion of host structure. *J. Phys. Chem. C* **2013**, *117*, 7081–7085. [CrossRef]
26. Chuvilin, E.; Bukhanov, B.; Davletshina, D.; Grebenkin, S.; Istomin, V. Dissociation and Self-Preservation of Gas Hydrates in Permafrost. *Geosciences* **2018**, *8*, 431. [CrossRef]
27. Podenko, L.S.; Drachuk, A.O.; Molokitina, N.S.; Nesterov, A.N. Effect of silica nanoparticles on dry water gas hydrate formation and self-preservation efficiency. *Zhurnal Fiz. Khimii* **2018**, *92*, 239–246. (In Russian) [CrossRef]
28. Yakushev, V.S. Mechanisms of natural gas concentration in the cryolithozone. *Actual Probl. Oil Gas* **2018**, *4*, 71. [CrossRef]

29. Nikitin, V.V.; Dugarov, G.A.; Duchkov, A.A.; Fokin, M.I.; Drobchik, A.N.; Shevchenko, P.D.; Francesco De, C.; Rajmund, M. Dynamic in-situ imaging of methane hydrate formation and self-preservation in porous media. *Mar. Pet. Geol.* **2020**, *115*, 104234. [CrossRef]

30. Takeya, S.; Ebinuma, T.; Uchida, T.; Nagao, J.; Narita, H. Self-preservation effect and dissociation rates of CH_4 hydrate. *J. Cryst. Growth* **2002**, *237*, 379–382. [CrossRef]

31. Takeya, S.; Uchida, T.; Nagao, J.; Ohmura, R.; Shimada, W.; Kamata, Y.; Ebinuma, H.; Narita, H. Particle size effect of CH_4 hydrate for self-preservation. *Chemecal Eng. Sci.* **2005**, *60*, 1383–1387. [CrossRef]

32. Takeya, S.; Yoneyama, A.; Ueda, K.; Mimachi, H.; Takahashi, M.; Sano, K.; Hyodo, K.; Takeda, T.; Gotoh, Y. Anomalously preserved clathrate hydrate of natural gas in pellet form at 253 K. *J. Phys. Chem. C* **2012**, *116*, 13842–13848. [CrossRef]

33. Takeya, S.; Mimachi, H.; Murayama, T. Methane storage in water frameworks: Self-preservation of methane hydrate pellets formed from NaCl solutions. *Appl. Energy* **2018**, *230*, 86–93. [CrossRef]

34. Kuhs, W.F.; Genov, G.; Staykova, D.K.; Hansen, T. Ice perfection and onset of anomalous preservation of gas hydrates. *Phys. Chem. Chem. Phys.* **2004**, *6*, 4917–4920. [CrossRef]

35. Shimada, W.; Takeya, S.; Kamata, Y.; Uchida, T.; Nagao, J.; Ebinuma, T.; Narita, H. Mechanism of self-preservation during dissociation of methane clathrate hydrate. In Proceedings of the 5th International Conference on Gas Hydrate, Trondheim, Norway, 13–16 June 2005.

36. Falenty, A.; Kuhs, W.F. "Self-Preservation" of CO_2 Gas Hydratess Surface Microstructure and Ice Perfection. *J. Phys. Chem. B* **2009**, *113*, 15975–15988. [CrossRef]

37. Melnikov, V.P.; Nesterov, A.N.; Reshetnikov, A.M.; Zavodovsky, A.G. Evidence of liquid water formation during methane hydrates dissociation below the ice point. *Chem. Eng. Sci.* **2009**, *64*, 1160–1166. [CrossRef]

38. Melnikov, V.P.; Nesterov, A.N.; Reshetnikov, A.M.; Istomin, V.A. Metastable states during dissociation of carbon dioxide hydrates below 273 K. *Chem. Eng. Sci.* **2011**, *66*, 73–77. [CrossRef]

39. Takeya, S.; Ripmeester, J.A. Anomalous Preservation of CH_4 hydrate and its dependence on the morphology of hexagonal ice. *Phys. Chem. Chem. Phys.* **2010**, *11*, 70–73. [CrossRef]

40. Ohno, H.; Nishimura, O.; Suzuki, K.; Narita, H.; Nagao, J. Morphological and compositional characterization of self-preserved gas hydrates by low-vacuum scanning electron microscopy. *Chem. Phys. Chem.* **2011**, *12*, 1661–1665. [CrossRef] [PubMed]

41. Uchida, T.; Kida, M.; Nagao, J. Dissociation termination of methane–ethane hydrates in temperature-ramping tests at atmospheric pressure below the melting point of ice. *Chem. Phys. Chem.* **2011**, *12*, 1652–1656. [CrossRef] [PubMed]

42. Nguyen, A.H.; Koc, M.A.; Shepherd, T.D.; Molinero, V. Structure of the Ice–Clathrate Interface. *J. Phys. Chem. C* **2015**, *119*, 4104–4117. [CrossRef]

43. Zhong, J.-R.; Zeng, X.-Y.; Zhou, F.-H.; Ran, Q.-D.; Sun, C.-Y.; Zhong, R.-Q.; Yang, L.-Y.; Chen, G.-J.; Koh, C.A. Self-preservation and structural transition of gas hydrates during dissociation below the ice point: An in-situ study using Raman spectroscopy. *Sci. Rep.* **2016**, *6*, 13. [CrossRef]

44. Mimachi, H.; Takeya, S.; Yoneyama, A.; Hyodo, K.; Takeda, T.; Gotoh, Y.; Murayama, T. Natural gas storage and transportation within gas hydrate of smaller particle: Size dependence of self-preservation phenomenon of natural gas hydrate. *Chem. Eng. Sci.* **2014**, *118*, 208–213. [CrossRef]

45. Prasad, P.S.R.; Kiran, B.S. Self-preservation and Stability of Methane Hydrates in the Presence of NaCl. *Sci. Rep.* **2019**, *9*, 5860. [CrossRef]

46. Stoporev, A.S.; Manakov, A.Y.; Altunina, L.K.; Strelets, L.A. Self-Preservation of Gas Hydrate Particles Suspended in Crude Oils and Liquid Hydrocarbons: Role of Preparation Method, Dispersion Media, and Hydrate Former. *Energy Fuels* **2016**, *3011*, 9014–9021. [CrossRef]

47. Kuhs, W.F.; Staykova, D.K.; Salamatin, A.N. Formation of methane hydrate from polydisperse ice powders. *Phys. Chem. B* **2006**, *110*, 13283–13295. [CrossRef]

48. Ershov, E.D.; Yakushev, V.S.; Chuvilin, E.M. Laboratory studies of frozen natural and artificial hydrate-bearing rock samples. In Proceedings of the 2th International Conference on Gas Hydrate, France, Toulouse, 2–6 June 1996; pp. 525–531.

49. Minagawa, H.; Ohmura, R.; Kamata, Y. Water permeability measurements of gas hydrate-bearing sediments. In Proceedings of the Fifth International Conference on Gas Hydrates, Trondheim, Norway, 13–16 June 2005; Tapir Academic Press: Trondheim, Norway, 2005; pp. 398–401.

50. Murray, D.; Fukuhara, M.; Khong, C.K.; Namikawa, T.; Yamamoto, K. Permeability estimates in gas hydrate reservoirs of the Nankai trough. In Proceedings of the SPWLA 47th Annual Logging Symposium, Veracruz, Mexico, 4–7 June 2006; pp. 1–6.

51. Kumar, A.; Maini, B.; Bishnoi, P.R.; Clarke, M.; Zatsepina, O.; Srinivasan, S. Experimental determination of permeability in the presence of hydrates and its effect on the dissociation characteristics of gas hydrates in porous media. *J. Pet. Sci. Eng.* **2010**, *70*, 114–122. [CrossRef]

52. Miyazaki, K.; Masui, A.; Sakamoto, Y.; Aoki, K.; Tenma, N.; Yamaguchi, T. Triaxial compressive properties of artificial methane-hydrate-bearing sediment. *J. Geophys. Res.* **2011**, *116(B06102)*, 1–11. [CrossRef]

53. Hyodo, M.; Li, Y.; Yoneda, J.; Nakata, Y.; Yoshimoto, N.; Nishimura, A.; Song, Y. Mechanical behavior of gas-saturated methane hydrate-bearing sediments. *J. Geophys. Res. Solid Earth* **2013**, *118*, 5185–5194. [CrossRef]

54. Chuvilin, E.M.; Grebenkin, S.I. Gas permeability variations in gas-filled soils upon hydrate formation and freezing: An experimental study. *Kriosf. Zemli* **2015**, *19*, 67–74. (In Russian).

55. Santamarina, J.C.; Dai, S.; Terzariol, M.; Jang, J.; Waite, W.F.; Winters, W.J. Hydro-bio-geomechanical properties of hydrate bearing sediments from Nankai Trough. *Mar. Pet. Geol.* **2015**, *66*, 434–450. [CrossRef]

56. Yoneda, J.; Masui, A.; Konno, Y.; Jin, Y.; Egawa, K.; Kida, M. Mechanical properties of hydrate-bearing turbidite reservoir in the first gas production test site of the Eastern Nankai Trough. *Mar. Pet. Geol.* **2015**, *66*, 471–486. [CrossRef]

57. Li, Y.; Liu, W.; Zhu, Y.; Chen, Y.; Song, Y.; Li, Q. Mechanical behaviors of permafrost-associated methane hydrate-bearing sediments under different mining methods. *Appl. Energy* **2016**, *162*, 1627–1632. [CrossRef]

58. Chuvilin, E.M.; Bukhanov, B.A. Effect of hydrate accumulation conditions on thermal conductivity of gas-saturated soils. *Energy Fuels* **2017**, *31*, 5246–5254. [CrossRef]

59. Liu, Z.; Dai, S.; Ning, F.; Peng, L.; Wei, H.; Wei, C. Strength estimation for hydrate-bearing sediments from direct shear tests of hydrate-bearing sand and silt. *Geophys. Res. Lett.* **2018**, *45*, 715–723. [CrossRef]

60. Chuvilin, E.M.; Bukhanov, B.A.; Grebenkin, S.I.; Doroshin, V.V.; Iospa, A.V. Shear strength of frozen sand with dissociating pore methane hydrate: An experimental study. *Cold Reg. Sci. Technol.* **2018**, *153*, 101–105. [CrossRef]

61. Chuvilin, E.M.; Grebenkin, S.I.; Zhmaev, M. Gas Permeability Behavior in Frozen Sand Controlled by Formation and Dissociation of Pore Gas Hydrates. *Geosciences* **2022**, *12*, 321. [CrossRef]

62. Yang, J.; Hassanpouryouzband, A.; Tohidi, B.; Chuvilin, E.; Bukhanov, B.; Istomin, V.; Cheremisin, A. Gas hydrates in permafrost: Distinctive effect of gas hydrates and ice on the geomechanical properties of simulated hydrate-bearing permafrost sediments. *JGR Solid Earth* **2019**, *124*, 2551–2563. [CrossRef]

63. Chuvilin, E.M.; Guryeva, O.M. Experimental investigation of CO_2 gas hydrate formation in porous media of frozen and freezing sediments. *Kriosf. Zemli* **2009**, *13*, 70–79. (In Russian).

64. Chuvilin, E.M.; Davletshina, D.A.; Lupachik, M.V. Hydrate formation in frozen and thawing methane-saturated sediments. *Earth's Cryosphere* **2019**, *23*, 44–52. [CrossRef]

65. Davletshina, D.A.; Chuvilin, E.M. Estimation of potential gas hydrate formation in finely dispersed soils at negative temperatures: Experimental modeling. *Earth's Cryosphere* **2020**, *24*, 25–33.

66. Jahn, R.; Blume, H.P.; Spaargaren, O.; Schad, P. *Guidelines for Soil Description*; Food and Agriculture Organization of the United Nations: Rome, Italy, 2006.

67. Chuvilin, E.M.; Petrakova, S.Y.; Guryeva, O.M.; Istomin, V.A. Formation of carbon dioxide gas hydrates in freezing sediments and decomposition kinetics of the hydrates formed. In Proceedings of the 11th Intern. Conference, Physics and Chemistry of Ice, Cambridge, UK, 23–28 July 2007.

68. Minagawa, H.; Nishikawa, Y.; Ikeda, I.; Miyazaki, K.; Takahara, N.; Sakamoto, Y.; Komai, T.; Narita, H. Characterization of sand sediment by pore size distribution and permeability using proton nuclear magnetic resonance measurement. *J. Geophys. Res.* **2008**, *113*, B07210. [CrossRef]

69. Yang, M.; Chong, Z.R.; Zheng, J.; Song, Y.-C.; Linga, P. Advances in nuclear magnetic resonance (NMR) techniques for the investigation of clathrate hydrates. *Renew. Sustain. Energy Rev.* **2017**, *74*, 1346–1360. [CrossRef]

70. Zhan, J.; Zhang, P.; Wang, Y.; Wu, Q. Experimental research on methane hydrate formation in porous media based on the low-field NMR technique. *Chem. Eng. Sci.* **2021**, *244*, 116804. [CrossRef]

71. Ji, Y.K.; Liu, C.L.; Zhang, Z.; Meng, Q.G.; Liu, L.L.; Zhang, Y.C.; Wu, N.Y. Experimental study on characteristics of pore water conversion during methane hydrates formation in unsaturated sand. *China Geol.* **2022**, *5*, 276–284. [CrossRef]

72. Chuvilin, E.M.; Kozlova, E.V.; Petrakova, S.Y. Kinetics of gas hydrate dissociation in permafrost at negative temperatures. *Gazov. Promyshlennost* **2006**, 47–50. (In Russian).

73. Yershov, E. *General Geocryology (Studies in Polar Research)*; Williams, P., Ed.; Cambridge University Press: Cambridge, UK, 1998; p. 550. ISBN 9780521607575.

74. Chuvilin, E.M.; Bukhanov, B.A.; Mukhametdinova, A.Z.; Grechishcheva, E.S.; Alekseev, A.G.; Istomin, V.A. Freezing point and unfrozen water contents of permafrost soils: Estimation by the water potential method. *Cold Reg. Sci. Technol.* **2022**, *196*, 103488. [CrossRef]

75. Vlasov, V.A.; Zavodovsky, A.G.; Madygulov, M.S.; Reshetnikov, A.M. Formation of supercooled water on dissociation of gas hydrates, from nuclear magnetic resonance data. *Earth's Cryosphere* **2011**, *15*, 83–85.

76. Melnikov, V.P.; Nesterov, A.N.; Podenko, L.S.; Reshetnikov, A.M.; Shalamov, V.V. NMR evidence of supercooled water formation during gas hydrate dissociation below the melting point of ice. *Chem. Eng. Sci.* **2012**, *71*, 573. [CrossRef]

77. Zavodovsky, A.G.; Madygulov, M.S.; Reshetnikov, A.M. Equilibrium conditions and the region of metastable states of Freon-12 gas hydrate. *Russ. J. Phys. Chem.* **2015**, *89*, 2178–2182. [CrossRef]